EPJ Web of Conferences **314**, 00016 (2024) https://doi.org/10.1051/epjconf/202431400016
QCD@Work 2024

Effects of atomic electron momentum distribution on resonant dark sector production*

Fernando Arias-Aragón[1], *Luc* Darmè[2], *Giovanni* Grilli di Cortona[3,**], and *Enrico* Nardi[1,4]

[1]Istituto Nazionale di Fisica Nucleare, Laboratori Nazionali di Frascati, Frascati, 00044, Italy
[2]Université Claude Bernard Lyon 1, CNRS/IN2P3, Institut de Physique des 2 Infinis de Lyon, UMR 5822, F-69622, Villeurbanne, France
[3]Istituto Nazionale di Fisica Nucleare, Laboratori Nazionali del Gran Sasso, Assergi, 67100, L'Aquila (AQ), Italy
[4]Laboratory of High Energy and Computational Physic, HEPC-NICPB, Rävala 10, 10143, Tallin, Estonia

Abstract. Exploring resonant positron annihilation on atomic electrons offers a promising method for detecting light dark sector particles that interact with e^+e^- pairs. However, to accurately estimate production rates, a thorough understanding of atomic electron momentum distributions is essential. We introduce a comprehensive approach using the Compton profile of target materials to accurately incorporate electron velocity effects into resonant annihilation cross-sections. We show that taking into account the finite motion of atomic electrons not only can improve the search for new physics, but can also allow to enhance the accuracy of hadronic cross-section measurements.

1 Introduction

Compelling evidence for the existence of physics beyond the Standard Model is provided by established phenomena like neutrino masses, dark matter and the cosmological baryon asymmetry. New physics may manifest in a new sector with new particles and interactions. Intense positron beams impinging on fixed targets can be used to search for new light particles with feeble couplings to electrons and positrons. The power of this strategy relies on the fact that, if the condition for resonant e^+e^- annihilation into new states occurs, it would lead to a huge enhancement of the production rates [1, 2], a technique that is already being exploited by the experimental community [3, 4].

In experiments with thick fixed targets of large nuclear charge, a continuous scanning over the suitable centre-of-mass energy range can be achieved by keeping the beam energy fixed, as the positron will lose energy while passing through the target. On the other hand, in thin targets of low nuclear charge, the positron energy loss traversing the material is negligible and the beam energy must be tuned to span the desired range. In both cases, reliable estimates of resonant production rates and signal shapes can be obtained only after a careful characterization of the atomic electron momentum distribution.

*Presented by G. Grilli di Cortona at the QCD@Work: International Workshop on QCD, 18-21 June 2024, Trani, Italy

**e-mail: giovanni.grilli@lngs.infn.it

In this contribution, we discuss the impact of atomic electron momentum distribution on resonant dark sector production in fixed target experiments, presented in Ref. [5] (see also Ref [6]). Furthermore, we present a new method, discussed for the first time in Ref. [7], that can allow a measurement of the $e^+e^- \to$ hadrons cross-section leveraging the relativistic velocity of atomic electrons in targets with large atomic number Z.

2 Cross sections

In this section we discuss how to compute the cross section for the process $e^+e^- \to X$, where the particle X is resonantly produced, and for di-muon production. The latter process will allow us to obtain $\sigma_{\rm had} = \sigma(e^+e^- \to \text{hadrons}) = R(s)\,\sigma^{\rm th}_{\mu\mu}(s)$ via the experimentally measured R-ratio $R(s) = N_{\rm had}(s)/N_{\mu\mu}(s)$, where $N_{\mu\mu}$ denotes the number of di-muon events, while $N_{\rm had}$ is the number of hadronic events.

2.1 Resonant production

The differential cross section for positron annihilation off an atomic electron can be written as:

$$d\sigma_q = \frac{d^3p}{(2\pi)^3}\frac{d^3k_A}{(2\pi)^3}\frac{d^3k_B}{(2\pi)^3}\frac{(2\pi)^4\delta^{(4)}(\hat{k}_A+\hat{k}_B-\hat{p})}{2E_X 2E_{k_A} 2E_B\,|v_A - v_B|}\left|\phi_{A,q}(\boldsymbol{k}_A)\right|^2 |\mathcal{M}_{\rm free}|^2\,|\phi_B(\boldsymbol{k}_B)|^2 \tag{1}$$

where q collectively labels the orbital quantum numbers, the subscripts A and B denote respectively electron and positron quantities, and $\phi(\boldsymbol{k})$, $\boldsymbol{k}$ and E denote their wave function, momentum and energy respectively. The term $\delta^{(4)}(\hat{k}_A+\hat{k}_B-\hat{p}) = \delta^{(3)}(\boldsymbol{k}_A+\boldsymbol{k}_B-\boldsymbol{p})\delta(E_A+E_B-E_X)$ enforces three-momentum and energy conservation, with $E_A = m_e$ the atomic electron energy neglecting its binding energy. Finally, p and E_X denote the momentum and energy of the final X particle, while $E_{k_A} = \sqrt{k_A^2+m_e^2}$. Taking the positrons in the beam as free particles with a well defined momentum $\boldsymbol{p}_B$, its wave function satisfies: $\int \frac{dk_B^3}{(2\pi)^3}\,|\phi_B(\boldsymbol{k}_B)|^2 = 1$, and $|\phi_B(\boldsymbol{k}_B)|^2 = (2\pi)^3\delta^{(3)}(\boldsymbol{p}_B - \boldsymbol{k}_B)$. On the other hand, atomic electrons are confined in space, implying a certain probability distribution associated with their momenta. The electron momentum density function $n(\boldsymbol{k}_A)$ is normalised to the atomic number Z of the target atoms as follows

$$n(\boldsymbol{k}_A) = \sum_q \left|\phi_q(\boldsymbol{k}_A)\right|^2, \quad \int \frac{d^3k_A}{(2\pi)^3}\,n(\boldsymbol{k}_A) = Z\,. \tag{2}$$

The electron momentum density distribution $n(\boldsymbol{k}_A)$ will be discussed in detail in Section 2.3. Neglecting the binding energy and assuming isotropy of the atomic electron momentum distribution, we can sum (1) over q, perform the integration over d^3p, and finally obtain

$$\frac{d\sigma}{dk_A} = \frac{|\mathcal{M}_{\rm free}|^2}{16\pi}\,\frac{k_A\,n(k_A)}{p_B|E_B k_A x_0(k_A) - E_{k_A} p_B|}. \tag{3}$$

Energy conservation implies that

$$x_0(k_A) = \frac{2E_AE_B + 2m_e^2 - m_X^2 - k_A^2}{2k_Ap_B}, \quad k_A^{\rm max,min} = \left|p_B \pm \sqrt{(E_A+E_B)^2 - m_X^2}\right|. \tag{4}$$

The energy distribution of positrons in the beam, described by a Gaussian $\mathcal{G}(E,\,E_B,\,\sigma_B)$ centered at E_B and with a standard deviation σ_B, must be taken into account while computing the cross-section

$$\sigma(E_B,\,\sigma_B) = \int dE\,\mathcal{G}(E,\,E_B,\,\sigma_B)\,\sigma(E), \tag{5}$$

where $\sigma(E)$ is the cross-section obtained after integrating Eq. (3).

2.2 Di-muon production

The differential cross-section for the annihilation of a positron with an atomic electron in a certain orbital n, ℓ with momentum-space wave-function $\phi_{n\ell}(\boldsymbol{k}_A)$ is

$$d\sigma = \frac{d^3p_1 d^3p_2 d^3k_A}{(2\pi)^5 16 E_1 E_2} \frac{|\phi_{nl}(\boldsymbol{k}_A)|^2 \, |\mathcal{M}_{\rm free}|^2}{|E_B k_A^z - E_{k_A} p_B|} \delta^4(\hat{k}_A + \hat{p}_B - \hat{p}_f). \tag{6}$$

In (6), $\mathcal{M}_{\rm free}$ is the matrix element, and $\delta^{(4)}(\hat{k}_A + \hat{p}_B - \hat{p}_f) = \delta^{(3)}(\boldsymbol{k}_A + \boldsymbol{p}_B - \boldsymbol{p}_1 - \boldsymbol{p}_2)\delta(E_A + E_B - E_1 - E_2)$ denotes the three-momentum and energy conservation. We have neglected the electron binding energy in the energy conservation condition by setting $E_A = m_e$, justified by the separation of scales with the centre-of-mass (c.m.) energy in the process.

Performing all the integration, see Ref. [7] for more details, we finally obtain:

$$\frac{d^2\sigma}{ds\, dc_{\theta_2}} = \int_{m_\mu}^{\infty} dE_2 \int_0^{\infty} dk_A \, \frac{|\mathcal{M}_{\rm free}|^2}{32\pi^2} \, \frac{|\phi_{nl}(k_A)|^2}{16\pi^3} \, \frac{(2\pi - \arccos d)\,\Pi\left(\frac{d}{2}\right)}{p_B |E_B k_A c_{\theta_A} - E_{k_A} p_B|\, s_{\theta_2} s_{\theta_A} \sqrt{1-d^2}}, \tag{7}$$

with

$$\begin{aligned} d &= \frac{a - \mathcal{E}^2}{b}, \\ a &= p_2^2 + m_\mu^2 + k_A^2 + p_B^2 + 2k_A p_B c_{\theta_A} - 2p_2 c_{\theta_2}(p_B + k_A c_{\theta_A}), \qquad b = 2k_A p_2 s_{\theta_2} s_{\theta_A}, \\ \mathcal{E} &= E_A + E_B - E_2. \end{aligned} \tag{8}$$

In (7) we assumed an isotropic distribution for the electron momentum, and used spherical coordinates $d^3k_A = k_A^2 dk_A dc_{\theta_A} d\varphi_A$ and $d^3p_2 = p_2^2 dp_2\, dc_{\theta_2} d\varphi_2$, where $c_{\theta_A} = \cos\theta_A$ and $c_{\theta_2} = \cos\theta_2$. Moreover the Π function restricts the integration to values for which $|d| < 1$ and enforces energy conservation. Furthermore, $c_{\theta_A} = (2m_e^2 + 2E_A E_B - s - k_A^2)/(2p_B k_A)$.

2.3 Atomic electron momentum distribution

A fundamental aspect in the cross-section calculation is the electron momentum distribution $n(k_A)$. This quantity can be directly extracted from measurements of the Compton profile (CP) [8]. The electron momentum density from spherically averaged Compton profiles is defined as [9]

$$J(p) = \frac{1}{2} \int_{|p|}^{\infty} \rho(k) k dk, \tag{9}$$

with $\rho(k)$ the electron momentum distribution, and it is normalised as $\int_{-\infty}^{\infty} J(p)dp = Z$. In our notation, this implies that $\rho(k) = \frac{n(k)}{2\pi^2}$ and the electron momentum density distribution is

$$n(k) = -\frac{(2\pi)^2}{k} \frac{dJ(k)}{dk}. \tag{10}$$

In Fig. 1 we show the comparison between cross sections for the resonant process $e^+e^- \to X$ evaluated as a function of the beam energy, where X is a vector particle with mass m_X and interaction with electrons described by $\mathcal{L}_X \subset g_V X_\mu \bar{e}\gamma^\mu e$. We discuss the results for two targets: diamond, as it is used by the PADME Collaboration in the search for the X_{17} boson [10–12], and tungsten, as an example of a large-Z material. The results for the diamond target are given in the left panel of Fig. 1, where the blue curve is obtained under the assumption of atomic electrons at rest, so that the broadening of the curve is entirely due

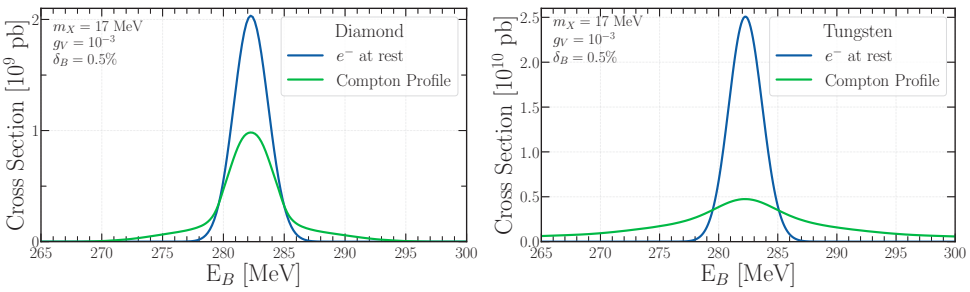

Figure 1. Resonant production cross section for a new vector boson with mass $m_X = 17$ MeV and coupling $g_V = 10^{-3}$, including the effects of a 0.5% beam energy spread, for a diamond (left) and a tungsten (right) target. The blue curve assumes electrons at rest, while the green one accounts for the atomic electron momentum distribution via the CP.

to the beam energy spread. The green curve, on the other hand, is obtained using the CP from Ref. [9]. This last curve is more spread due to the atomic electron motion. The particular shape of the green curve is due to the fact that the four atomic electrons belonging to the valence shells contribute to the central peak, while the two core electrons contribute to the broader tails.

The right panel shows the same result for tungsten, where the larger momentum of core electrons leads to a more significant energy spread. As a consequence, in both cases the smearing of the resonance has an important effect on searches for resonant peaks at fixed target experiments.

3 Atoms as electron accelerators

The motion of atomic electrons has a strong impact on the production of light new bosons via electron-positron resonant annihilation. In the following, we will focus on searches for light dark sector particles, in particular the X_{17} [10–15]. Finally, we propose to measure the cross-section for $e^+e^- \to$ hadrons at experiments where positron beams scatter on fixed targets [7], taking advantage of the atomic electron momentum distribution to scan the relevant energy range.

3.1 Impact on new physics searches

Resonantly produced vector bosons, a possible explanation of the ATOMKI anomaly [13–15], are affected by the target electron motion. Figure 2 shows the sensitivity of the PADME experiment to the X_{17} particle mass and coupling, assuming a 12 energy bin scan in the range $E_B = [265, 297]$ MeV, using $6 \cdot 10^{11}$ total positron on a 100 μm diamond target and with a beam energy spread of 0.5%.[1] The gray areas are excluded by several experiments [16–20]. The shaded violet regions show the 1σ and 2σ range for $m_X \sim 16.98 \pm 0.21$ MeV, obtained by combining the statistical uncertainties from the ATOMKI measurements [13–15] and adding in quadrature a systematic error of 0.20 MeV. The result obtained by assuming electrons at rest is depicted by the blue dashed line [12]. Finally, the projected sensitivity including the electron velocity effects via the CP is shown by the orange solid line. These last two curves were obtained by assuming $\sim 7.5 \times 10^4$ background events from Bhabha scattering and

[1] For the actual strategy employed by the PADME Collaboration, see [4].

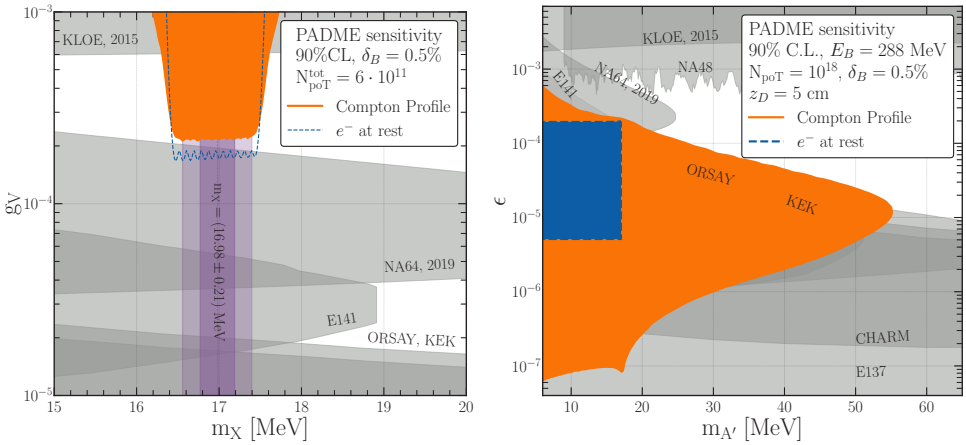

Figure 2. Projected sensitivity of the PADME run-III (left) on g_V as a function of the X_{17} mass and on the dark photon kinetic mixing ϵ as a function of the dark photon mass (right). Figures from [5].

neglecting the $\gamma\gamma$ background. In this analysis, systematic uncertainties have been neglected. As a result, correctly accounting for the atomic electron momentum distribution leads to a certain loss in sensitivity because the signal gets distributed over a broader range of energies, reducing the signal-to-noise ratio.

Taking advantage of the atomic electron motion gives also an opportunity to probe larger masses. In fact, the atomic electron motion can increase the centre of mass energy of the collision. The right panel of Figure 2 shows the exclusion limits for dark photon searches where the dark photon decays only to an electron-positron pair with coupling $\epsilon = g_V/e$. The gray regions represent the exclusion limits from several experiments [16, 17, 19–24]. The orange shaded area shows the 2.7 event limit (corresponding to 90% C.L.) that can be reached at an experiment with a positron beam with $E_B = 288$ MeV scattering on a 5 cm-thick tungsten target, assuming 10^{18} positrons on target and no background. The larger mass reach with respect to the blue region obtained assuming target electron at rest is due to the contribution of atomic electrons with large momenta.

3.2 A proposal for measuring the hadronic cross section

The large momenta of the core electron of high-Z materials can be used to precisely measure the hadronic cross section. A suitable positron beam is the one from the CEBAF facility at Jefferson Lab (JLab). The JLab injector could produce $1 - 5\,\mu$A unpolarized positron beams accelerated up to energies of 12 GeV, with a negligible energy spread. One year of data taking could produce up to 10^{21} positrons on target. This could be enough to measure a large number of di-muon events, as shown by the blue line of Figure 3 left, by scattering 10^{21} positrons of $E_B = 12$ GeV on a 500 μm uranium target.[2] This result is compared to the $\mu\mu\gamma$ events detected by KLOE [25]. The Figure shows that JLAB has the potential to collect more statistics than KLOE even at c.m. energies of order 1 GeV.

Furthermore, at CERN positron beams of energy between 100 and 200 GeV are available. It is, therefore, natural to ask how an increase in energy would change this measurement.

[2] We chose uranium as a target since it has the largest momentum spread in its core electrons. Other heavy targets, like tungsten, would give a weaker but comparable result.

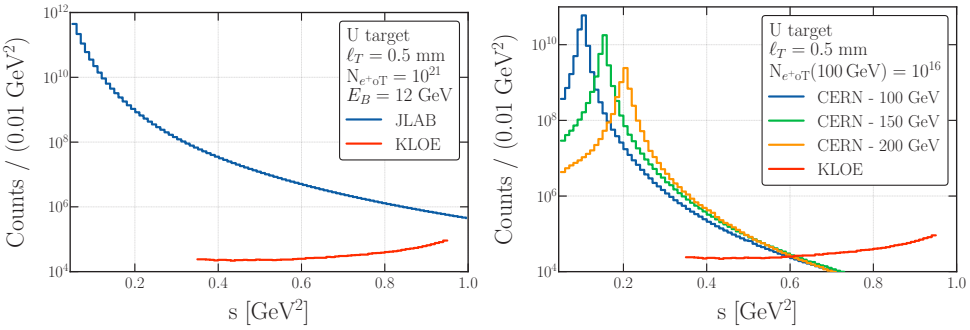

Figure 3. Left: number of $\mu\mu$ events produced at JLAB (blue) with a 12 GeV beam energy, compared to the di-muon events measured in KLOE [25]. Right: number of $\mu\mu$ events produced at CERN beam line (blue, green and orange) with a 100, 150 and 200 GeV beam energy, compared to the di-muon events measured in KLOE [25]. Figures from [7].

Those beams, however, may reach a statistics of $\sim 6.5{\cdot}10^{12}\, e^+$oT/yr for a 100 GeV beam. This is not sufficient to allow for a useful measurement, as shown in the right panel of Figure 3. We explore nevertheless the energy dependence of the measurement by assuming an (unrealistic) $N_{e^+\text{oT}} \sim 10^{16}$ for a beam energy $E_B = 100\,\text{GeV}$ and a $500\,\mu$m uranium target. We account for the scaling of the beam intensity at $E_B > 100\,\text{GeV}$ by using the following parametrization $N_{e^+\text{oT}}(p') = N_{e^+\text{oT}}(p) e^{-\frac{B}{p_0}(p'-p)}$, where p_0 is the energy of the primary protons (400 GeV), $B = 10$, and $N_{e^+\text{oT}}(100\,\text{GeV}) = 10^{16}$ [26]. These results are shown in the right panel of Fig. 3 for $E_B = 100$, 150, 200 GeV (blue, green and orange histogram, respectively). The red histogram shows the $\mu\mu\gamma$ events from KLOE. Above $s \sim 0.6$ GeV^2 an increase in the beam energy does not lead to an improvement of the statistics: the decrease in beam intensity offsets the advantage of increasing the beam energy. Therefore, considering the larger hadron contamination at higher energy, lower beam energies are preferable.

4 Conclusions

We showed the impact of atomic electron momentum distribution in new physics searches at fixed target experiments. In particular, we showed that the high momentum of core electron in large-Z materials can improve the mass reach in models of dark photons with couplings only to e^+e^- pairs. Finally, we proposed a novel strategy to measure the hadronic cross section. This could play a crucial role in solving the issues in the determinations of the hadron vacuum polarization contribution to the muon anomalous magnetic moment extracted from $e^+e^- \to$ hadrons data, and could rule out possible new physics explanations of the disagreement [27, 28].

G.G.d.C received partial financial support by the INFN "Iniziativa specifica" PADME@LNF. The work of E.N. was supported by the Estonian Research Council grant PRG1884.

References

[1] E. Nardi, Dark Photon production in positron beam dump experiments via resonant annihilation, in *New directions in Dark Matter and Neutrino Physics,* Perimeter Institute, July 20-22, 2017, (PI Video Library: http://pirsa.org/17070015) (2017)

[2] E. Nardi, C.D.R. Carvajal, A. Ghoshal, D. Meloni, M. Raggi, Resonant production of dark photons in positron beam dump experiments, Phys. Rev. D **97**, 095004 (2018), 1802.04756. 10.1103/PhysRevD.97.095004

[3] Y.M. Andreev et al., Improved exclusion limit for light dark matter from e+e- annihilation in NA64, Phys. Rev. D **104**, L091701 (2021), 2108.04195. 10.1103/PhysRevD.104.L091701

[4] PADME Collaboration, in preparation (2024)

[5] F. Arias-Aragón, L. Darmé, G. Grilli di Cortona, E. Nardi, Production of Dark Sector Particles via Resonant Positron Annihilation on Atomic Electrons, Phys. Rev. Lett. **132**, 261801 (2024), 2403.15387. 10.1103/PhysRevLett.132.261801

[6] R. Plestid, M.B. Wise, Atomic binding corrections for high energy fixed target experiments (2024), 2403.12184

[7] F. Arias-Aragón, L. Darmé, G. Grilli di Cortona, E. Nardi, Atoms as electron accelerators for measuring the $e^+e^- \to$ hadrons cross section (2024), 2407.15941

[8] M.J. Cooper, Compton scattering and electron momentum determination, Reports on Progress in Physics **48**, 415 (1985). 10.1088/0034-4885/48/4/001

[9] J.C. Aguiar, C.R. Quevedo, J.M. Gomez, H.O. Di Rocco, Theoretical Compton profile of diamond, boron nitride and carbon nitride, Physica B Condensed Matter **521**, 361 (2017). 10.1016/j.physb.2017.07.016

[10] M. Raggi, V. Kozhuharov, Proposal to Search for a Dark Photon in Positron on Target Collisions at DAΦNE Linac, Adv. High Energy Phys. **2014**, 959802 (2014), 1403.3041. 10.1155/2014/959802

[11] M. Raggi, V. Kozhuharov, P. Valente, The PADME experiment at LNF, EPJ Web Conf. **96**, 01025 (2015), 1501.01867. 10.1051/epjconf/20159601025

[12] L. Darmé, M. Mancini, E. Nardi, M. Raggi, Resonant search for the X17 boson at PADME, Phys. Rev. D **106**, 115036 (2022), 2209.09261. 10.1103/PhysRevD.106.115036

[13] A.J. Krasznahorkay et al., Observation of Anomalous Internal Pair Creation in Be8 : A Possible Indication of a Light, Neutral Boson, Phys. Rev. Lett. **116**, 042501 (2016), 1504.01527. 10.1103/PhysRevLett.116.042501

[14] A.J. Krasznahorkay et al., New results on the ^{8}Be anomaly, J. Phys. Conf. Ser. **1056**, 012028 (2018). 10.1088/1742-6596/1056/1/012028

[15] A.J. Krasznahorkay, M. Csatlós, L. Csige, J. Gulyás, A. Krasznahorkay, B.M. Nyakó, I. Rajta, J. Timár, I. Vajda, N.J. Sas, New anomaly observed in He4 supports the existence of the hypothetical X17 particle, Phys. Rev. C **104**, 044003 (2021), 2104.10075. 10.1103/PhysRevC.104.044003

[16] M. Davier, H. Nguyen Ngoc, An Unambiguous Search for a Light Higgs Boson, Phys. Lett. B **229**, 150 (1989). 10.1016/0370-2693(89)90174-3

[17] A. Konaka et al., Search for Neutral Particles in Electron Beam Dump Experiment, Phys. Rev. Lett. **57**, 659 (1986). 10.1103/PhysRevLett.57.659

[18] Y.M. Andreev et al. (NA64), Search for pseudoscalar bosons decaying into e^+e^- pairs in the NA64 experiment at the CERN SPS, Phys. Rev. D **104**, L111102 (2021), 2104.13342. 10.1103/PhysRevD.104.L111102

[19] E.M. Riordan et al., A Search for Short Lived Axions in an Electron Beam Dump Experiment, Phys. Rev. Lett. **59**, 755 (1987). 10.1103/PhysRevLett.59.755

[20] A. Anastasi et al., Limit on the production of a low-mass vector boson in $e^+e^- \to U\gamma$, $U \to e^+e^-$ with the KLOE experiment, Phys. Lett. B **750**, 633 (2015), 1509.00740. 10.1016/j.physletb.2015.10.003

[21] Y.D. Tsai, P. deNiverville, M.X. Liu, Dark Photon and Muon $g-2$ Inspired Inelastic Dark Matter Models at the High-Energy Intensity Frontier, Phys. Rev. Lett. **126**, 181801 (2021), 1908.07525. 10.1103/PhysRevLett.126.181801

[22] S. Andreas, C. Niebuhr, A. Ringwald, New Limits on Hidden Photons from Past Electron Beam Dumps, Phys. Rev. D **86**, 095019 (2012), 1209.6083. 10.1103/PhysRevD.86.095019

[23] L. Marsicano, M. Battaglieri, M. Bondi', C.D.R. Carvajal, A. Celentano, M. De Napoli, R. De Vita, E. Nardi, M. Raggi, P. Valente, Dark photon production through positron annihilation in beam-dump experiments, Phys. Rev. D **98**, 015031 (2018), 1802.03794. 10.1103/PhysRevD.98.015031

[24] E. Depero et al. (NA64), Hunting down the X17 boson at the CERN SPS, Eur. Phys. J. C **80**, 1159 (2020), 2009.02756. 10.1140/epjc/s10052-020-08725-x

[25] D. Babusci et al. (KLOE), Precision measurement of $\sigma(e^+e^- \to \pi^+\pi^-\gamma)/\sigma(e^+e^- \to \mu^+\mu^-\gamma)$ and determination of the $\pi^+\pi^-$ contribution to the muon anomaly with the KLOE detector, Phys. Lett. B **720**, 336 (2013), 1212.4524. 10.1016/j.physletb.2013.02.029

[26] L. Gatignon, Design and Tuning of Secondary Beamlines in the CERN North and East Areas (2020). 10.17181/CERN.T6FT.6UDG

[27] L. Darmé, G. Grilli di Cortona, E. Nardi, The muon g − 2 anomaly confronts new physics in e and μ final states scattering, JHEP **06**, 122 (2022), 2112.09139. 10.1007/JHEP06(2022)122

[28] L. Darmé, G. Grilli di Cortona, E. Nardi, Indirect new physics effects on σhad confront the (g-2)μ window discrepancies and the CMD-3 result, Phys. Rev. D **108**, 095056 (2023), 2212.03877. 10.1103/PhysRevD.108.095056